ACS APPLIED MATERIALS & INTERFACES

Research Article

Cite This: ACS Appl. Mater. Interfaces 2019, 11, 40758−40768

www.acsami.org

Mechanical-Induced Polarization Switching in Relaxor Ferroelectric Single Crystals

Jihong Bian,[†] Yuting Wang,[†] Ren Zhu,[‡] Lei Wang,[†] Bian Yang,[†] Jianwei Wang,[†] Dawei Zhang,[§] Congcong Xu,[†] Tao Li,[∥] Dwight Viehland,[⊥] and Yaodong Yang*[,†]

[†]Frontier Institute of Science and Technology, State Key Laboratory for Mechanical Behavior of Materials, Xi'an Jiaotong University, Xi'an 710049, China

[‡]Oxford Instruments, No. 461 Hongcao Road, Shanghai 200233, China

[§]School of Materials Science and Engineering, University of New South Wales, Sydney, New South Wales 2052, Australia

[∥]Center for Spintronics and Quantum Systems, State Key Laboratory for Mechanical Behavior of Materials, Department of Materials Science and Engineering, Xi'an Jiaotong University, Xi'an, Shaanxi 710049, China

[⊥]Department of Materials Science and Engineering, Virginia Tech, Blacksburg, Virginia 24061, United States

Supporting Information

ABSTRACT: Control of coupling between electric and elastic orders in ferroelectric bulks is vital to understand their nature and enrich the multifunctionality of polarization manipulation applied in domain-based electronic devices such as ferroelectric memories and data storage ones. Herein, taking $(1 - x\%)Pb(Mg_{1/3}Nb_{2/3})O_3-x\%PbTiO_3$ (PMN−x%PT, x = 32, 40) as the prototype, we demonstrate the less-explored mechanical switching in relaxor ferroelectric single crystals using scanning probe microscopy. Low mechanical forces can induce metastable and electrically erasable polarization reversal clearly from electrical-created bipolar domains around the 180° domain wall in monoclinic PMN−32%PT and inside the c+ domain in tetragonal PMN−40%PT. The mechanical switching evolutions show force/time dependence and time-force equivalence. The time-dependent mechanical switching behavior stems from the participation and contribution of polar nanoregions. Flexoelectricity and bulk Vegard strain effect can account for the mechanical switching but notably, the former in the two has very different origins. These investigations exhibit the possibility of mechanical switching as a tool to manipulate polarization states in ferroelectric bulks, and provide the potential of these crystals as substrates in mechanical polarization control of future thin-film devices.

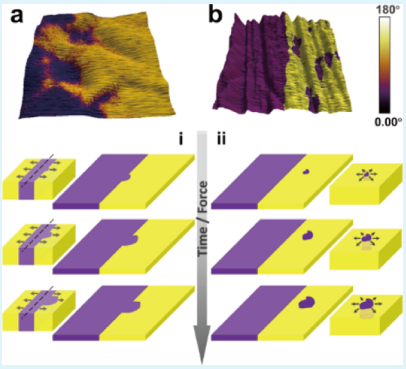

KEYWORDS: *mechanical switching, relaxor ferroelectrics, single crystal, flexoelectricity, scanning probe microscopy*

1. INTRODUCTION

Ferroelectrics are widely applied in random access memories[1] and data storage devices,[2] as well as actuators and transducers owing to their switchable polarization[3] and large piezoelectric constant. The electrical-induced polarization switching, reported to be one effective control coupled with other couplings such as the magnetic one exciting application potentials in future memory devices,[4,5] has been clearly described and well understood by plenty of experimental and theoretical studies[3,6−9] in the past decades. Recently, facilitated by advanced scanning probe microscopy (SPM),[7] polarization manipulation in response to stress stimuli[10] leads to intriguing phenomena[11] in ferroelectrics and multiferroics, endowing them the ability to control polarization and local order parameters under various fields for strain-couple device making and domain pattern writing, and thus attracts much attention for novel applications.

Although owning equal significance as the electrical-induced one, mechanical-induced polarization switching, however, has been less explored. It is notable that strain states cannot be changed by 180° ferroelectric switching but by non-180° switching.[12] As a result, ferroelastic switching is performed for strain-mediated coupling or strain-induced electronic devices. At the beginning, this strain-coupled polarization switching is still controlled electrically by applying voltages to the SPM probe in its lateral motion. Then, a groundbreaking switchable polarization generated by the stress gradient via mechanical writing from a scanning tip[13] directly indeed opens up explorations of pressure-induced surface phenomena in ferroelectrics and enables nonvolatile mechanical writing of large-area patterns for ferroelectric memories. Afterward, deterministic control[14] promotes the feasibility of mechanical switching in application.[15] However, the mechanical-induced

Received: July 13, 2019
Accepted: October 8, 2019
Published: October 8, 2019

DOI: 10.1021/acsami.9b12301
ACS Appl. Mater. Interfaces 2019, 11, 40758−40768

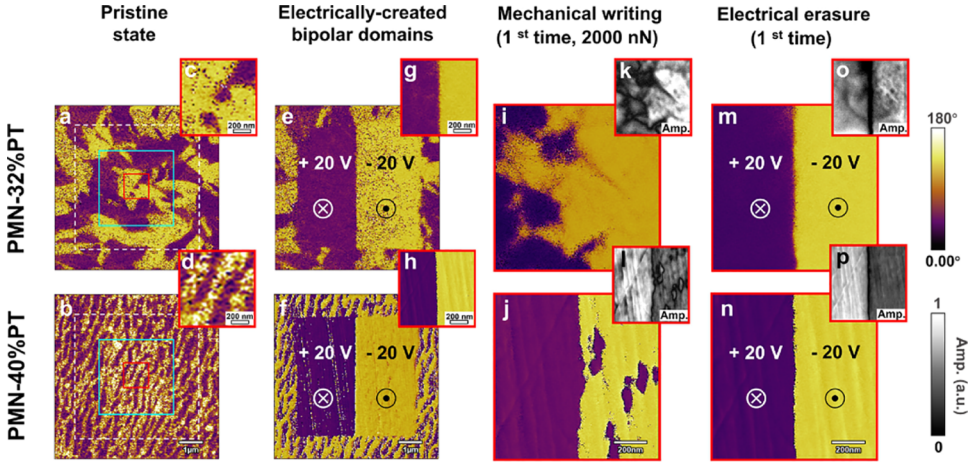

Figure 1. (a–d) Pristine, (e–h) electrical-created bipolar, (i–l) mechanical-written, and (m–p) electrical-erased domains in (100)-oriented PMN–32%PT and PMN–40%PT single crystals by PFM. PFM phase images of pristine domains over (a,b) 7 μm × 7 μm and (c,d) the central 1 μm × 1 μm (red squares in a,b) in the two crystals. PFM phase images of the central 5 μm × 5 μm (white dashed squares in a,b) electrical-created bipolar domains shown in (e,f) 7 μm × 7 μm and (g,h) 1 μm × 1 μm. PFM (i,j) phase and (k,l) amplitude images of mechanically switched domain patterns on 1 μm × 1 μm under a force of 2000 nN applied to the central 3 μm × 3 μm [cyan squares in (a,b)] from the electrical-created bipolar domains. In situ electrical-erasure of mechanical-induced domain patterns on the central 1 μm × 1 μm: PFM (m,n) phase and (o,p) amplitude images.

polarization switching is much more complex than the electrical one and controversy exists on its origin.

Many early reports attribute the switching to flexoelectricity,[13,16] a coupling between electric polarization and strain gradients. Afterward, the controversy remains as all the three effects are possible reasons,[17] that is, polarization rotation and suppression, strain gradient via flexoelectricity,[18] and surface or bulk electrochemical phenomena[19] related to vacancies.[20,21] Recently, the magnitudes of these effects are claimed to be remarkably close by phase-field modeling,[17] where the polarization field, flexoelectric strength, and vacancy concentration couple and interact. Accordingly, simulations have been recently developed by various techniques such as phase-field modeling,[17,22] molecular dynamics simulation,[23] and first-principles calculations[24] in similar systems, attempting to figure out the mechanisms of polarization reversal by stress. Moreover, it has been proposed that the mechanically induced 180° switching is driven by different mechanisms depending on thickness. In ultrathin films (thickness < 10 nm, especially < 5 nm), the surface chemical effect is in dominant; in thin films with a thickness of 10–20 nm, it is controlled by flexoelectric effect; and in thick films (thickness > 20 nm), the bulk oxygen vacancy-induced Vegard strain effect takes over.[17] Very recently, mechanical writing-direction-dependent asymmetric phenomena have been observed in experiments and analyzed by simulated results in c-oriented epitaxial $PbTiO_3$[25] and $BiFeO_3$[23] thin films, indicating the complexity of the mechanical switching process. Consequently, mechanisms of pressure-induced polarization switching are still under heated and intensive discussion up to date, ranging from polarization rotation and suppression, to flexoelectricity, and to complex surface electrochemical phenomena. The combination effect of these multiple factors leads to complex coupling between strain gradient, electric dipoles, and surface screening, and thus adds difficulties in mechanism clarifying.

Besides, mechanically induced polarization switching in low symmetry[18] ferroelectrics in various forms such as bulks[16] has little been achieved experimentally or theoretically. The aforementioned stress-induced polarization reversals are aroused only in ferroelectric and multiferroic thin films with chemical simplicity in high symmetry so far as model studies, for instance, in $PbTiO_3$,[25,26] $PbZr_{1-x}Ti_xO_3$,[10,22,27] $BaTiO_3$,[13] and $BiFeO_3$.[28,29] Actually, quite a lot of ferroelectrics with excellent performance have complexity in chemical components, physical structure (e.g., perovskite), and low symmetry; take the famous "piezoelectric prince" relaxor ferroelectric $Pb(Mg_{1/3}Nb_{2/3})O_3$–$PbTiO_3$ (PMN–PT), which owns alarge piezo response, excellent piezoelectricity,[30] and high electromechanical coupling[31] but is with complex perovskite structures[32] in various symmetries, as an example. These complexity and multiple existing forms (e.g., bulks as ceramics or single crystals, fibers, particles), as well as difficulties in ultrathin film syntheses make the awareness of mechanical switching in ferroelectrics far from clear.

Moreover, despite their own importance in research and wide applications in electronic and optical-electric devices, PMN–PT single crystals can be utilized as substrates[27,30,33] for thin-film-based memory devices, providing multiple manipulation methods to control polarization rotation and realize multiferroicity[30,33] in ferroelectric or ferromagnetic films, through the changes of electronic structure, strain, or magnetization generated from the polarization states' alteration in PMN–PT. Inspired by the truth that substrate bending can result in flexoelectricity and thus invoke polarization imprint,[33] it can be predicted that more approaches will be acquired to adjust the polarization state of films, if more means such as mechanical ones to regulate polarization are explored in these ferroelectric bulks. Nevertheless, the local interaction between mechanical field and polarization in PMN–PT is barely reported. Additionally, the difficulty in inducing a strain gradient large enough[34] limits the discovery of mechanical switching in bulks, as flexoelectricity is in inverse proportion to the relaxation length and thus can be omitted in bulks.[16,22] Therefore, pressure-induced switching remains largely unexplored and its related research is still needed urgently.

Hence, in this work, we investigate the mechanical-induced polarization switching in relaxor ferroelectric single crystals by SPM, taking $(1 - x\%)Pb(Mg_{1/3}Nb_{2/3})O_3$–$x\%PbTiO_3$

DOI: 10.1021/acsami.9b12301
ACS Appl. Mater. Interfaces 2019, 11, 40758–40768

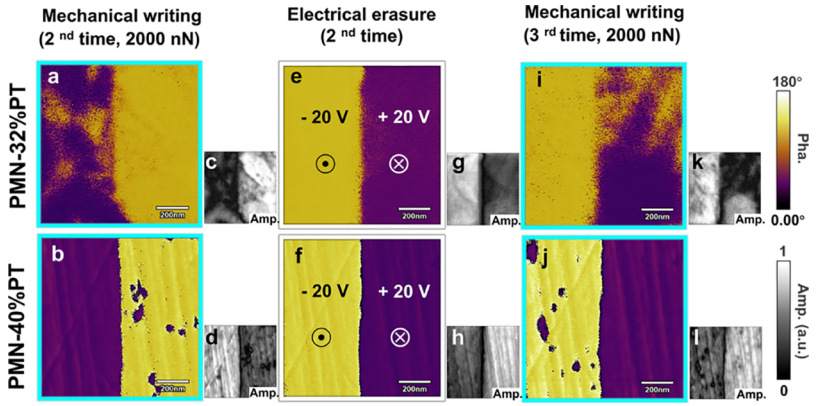

Figure 2. PFM phase and amplitude images of in situ domain configuration changes after mechanical switching for the second time in (a,c) PMN−32%PT and (b,d) PMN−40%PT, and after the second time electrical erasure in (e,g) PMN−32%PT and (f,h) PMN−40%PT, and after mechanical switching for the third time in (i,k) PMN−32%PT and (j,l) PMN−40%PT. Phase images are in color, whereas amplitude images are in black and white and labeled with "Amp.". Mechanical forces/electric voltages were applied to regions enclosed by cyan and white squares (1 μm × 1 μm), respectively.

(PMN−x%PT, x = 32, 40) single crystals in lower-symmetrical monoclinic structure and higher-symmetrical tetragonal structure, respectively, as prototypes. Their characteristic switching behaviors, together with dynamics and kinetics of domain evolution, are elaborated. The mechanisms of switching by mechanical forces are based on the flexoelectric effect and bulk Vegard strain effects. Our results help broaden the understanding of ferroelectrics in physics and nature, and reveal the possibility in device making by electrical/mechanical domain manipulation in future.

2. RESULTS AND DISCUSSION

2.1. Mechanical-Induced Polarization Switching Behaviors. Owing to their easy accessibility and definite correspondence between compositions and symmetry structures, in this study, we chose commercial (100)-oriented unpoled relaxor ferroelectric (1 − x%)Pb($Mg_{1/3}Nb_{2/3}$)O_3−x% $PbTiO_3$ (PMN−x%PT) (x = 32, 40) single crystals in thickness of 200 μm as research objects. The PMN−32%PT has a low-symmetric monoclinic (M) phase[32,35] and PMN−40%PT is in a high-symmetric tetragonal (T) phase.[32,36] Their piezoresponse force microscopy (PFM) phase, amplitude, and surface topography images of pristine domain structures within 7 μm × 7 μm are shown in Figures 1a,b and S1a,b and m,n, respectively. These domains have out-of-plane polarization and thus are c domains. At the very beginning, we applied mechanical forces directly to these domains. However, they remain the same (not shown) even under the maximum achievable load of 2000 nN by our SPM probe in this work. Considering the suggestion of writing a bipolar domain with an electrically biased PFM tip first to induce long-term stable domains[27] and the truth of the mechanical-induced switching aroused from electrical-poled bipolar patterns in ultrathin $BaTiO_3$ films[13] and 80 nm-in-thick $PbTiO_3$[25] films, we created such bipolar patterns over 5 μm × 5 μm (white dashed squares illustrated in Figure 1a,b) by electrical writing via litho PFM based on the same reason, as depicted in Figures 1e,f and S1e,f for the two crystals. In both specimens, c− domains (with out-of-plane polarization downward, in purple on the left) are separated by a 180° domain wall from c+ ones (with out-of-plane polarization upward, in yellow on the right). These electrical-created bipolar c domain patterns were utilized to investigate mechanical-induced polarization switching in the two crystals by a series of mechanical−electrical read−write experiments below. After writing by a mechanical force of 2000 nN from the tip over the central 3 μm × 3 μm regions (cyan squares illustrated in Figure 1a,b) in contact mode of atomic force microscopy (AFM), the central 1 μm × 1 μm (red squares in Figure 1a,b) bipolar domains (Figures 1c,d and S1c,d) change into patterns as illustrated in Figure 1i,k in PMN−32%PT and Figure 1j,l in PMN−40%PT. The PFM phase overlaid on the topography images of these two mechanically switched domain patterns are shown in Figure S2. In PMN−32%PT, the mechanical-induced polarization switching occurs in the vicinity of the 180° c domain wall. The wall moves to the left part with domains' reversal from c− to c + mainly. These switched domains are in a radius of ∼70−400 nm and in an area of ∼0.00385−0.115 μm^2. Consequently, the length and amount of the wall and area of c+ domains on the whole increase, whereas the area of the c− domain decreases. In PMN−40%PT, the mechanical-reversed domains mainly nucleate and grow inside the electrical-created c+ domain region from c+ into c−, whereas the original c− domain shows little response to the mechanical bias. These switched nanodomains are in a radius of ∼20−85 nm and in an area of ∼0.00177−0.0251 μm^2. In both cases, the mechanically switched domains can be erased thoroughly and easily by electrical switching (Figure 1m−p).

To investigate the characteristics and examine the repeatability of mechanical switching, we carried out in situ mechanical switching and electrical erasing for the other times (Figure 2). From Figure 2a−d, similar mentioned behaviors are observed in both single crystals for the second time switching; however, the overall mechanical-switched domain patterns vary a little except for the same nucleation spots as they did in the first switching experiment. From the results of mechanical switching and electrical erasure for the first two times, the mechanical domains can exist (Figure 1i,j) from the electrically polarized state (Figure 1g,h), and can be erased by electric stimuli (Figure 1m,n). Similar domains reoccur when the force was applied to the same regions under the same conditions (Figure 2a,b). Differences in the two times' mechanical writing may come from the tip erosion. Nevertheless, it is intriguing that the mechanically written domains seem to be reversible because of the same nucleation spots and similar domain patterns. These results may provide oppor-

DOI: 10.1021/acsami.9b12301
ACS Appl. Mater. Interfaces 2019, 11, 40758−40768

tunities for reversible control of polarization by electric and mechanical stimuli, which would be utilized for memory devices. Then, electrical dc voltages applied in the opposite way to the first time electrical erasure process lead to another entire erasure of these mechanically switched domains as shown in Figure 2e–h, resulting in c+ on the left and c− on the right. Afterward, mechanical-induced domain reversal for the third time obeys similar mechanical switching behaviors except for the very different nucleation spots inducing different patterns, in comparison with those in the first two switching processes. An overall view of 7 μm × 7 μm of the in situ mechanical switching for three times in PMN−32%PT is shown in Figure S3. Notably, the switching and growth of mechanically induced domains does not give rise to changes in topographies, suggesting that the switching process is nondestructive to the surface. These results reveal the repeatability, local-symmetry-dependence, writing-history-dependence of the mechanical-induced polarization switching which is nondestructive to the surface and erasable by electric dc bias thoroughly.

The mechanical-switched state in both the specimens above are illustrated in Figure 3a for PMN−32%PT (on 3 μm × 3 μm) and Figure 3c,d for PMN−40%PT (on 1 μm × 1 μm). Intriguingly, another mechanical switching state reversed from c+ to c− which is opposite to those shown in Figures 1 and 2 is visualized by the same aforementioned process at another spot in PMN−32%PT (Figure 3b). Still, these mechanically switched domains in PMN−32%PT gather around the electrical-created 180° c domain wall. Considering the areas away from the 180° domain wall, no clear c− domain reversal is observed in PMN−32%PT, in comparison to those visualized obviously inside the c+ domain in PMN−40%PT. Note that Figures 1e and S3a illustrate an overall view of in situ domain pattern changes in PMN−32%PT before and after the first mechanical switching where a force of 2000 nN was applied by the tip on the central area of 3 μm × 3 μm (shown in Figure S3a with the cyan square), respectively. It can be seen from Figure S3a that after the mechanical switching, only the central part around the domain wall changes obviously, whereas regions at the corners and sides of the cyan square, namely, areas inside the c− or c+ domain, away from the central 180° domain wall, hardly have any changes. We speculate that it is possible to switch single c− or c+ domains under larger forces. Under 2000 nN, from the current results, it is difficult to switch domains inside c− or c+ because of the requisite relative high nucleation energy inside c− or c+ than that near the 180° domain wall[37] in PMN−32%PT. To summarize, the mechanical force of 2000 nN can induce polarization switching in the vicinity of the 180° c domain wall from either c+ to c− or c− to c+ depending on location differences in PMN−32%PT, whereas it induces polarization switching inside electrical-created c+ domain from c+ to c− in PMN−40%PT.

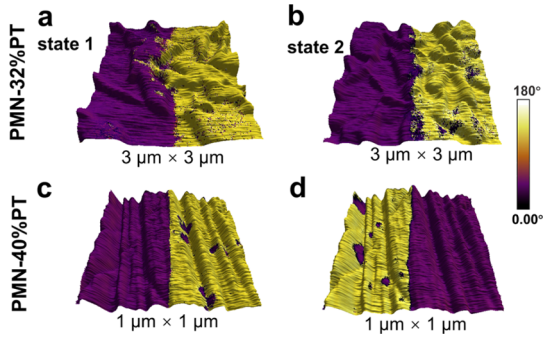

Figure 3. Visualized mechanical-induced polarization switching state by 2000 nN (a,b) at different spots on 3 μm × 3 μm in PMN−32%PT and (c,d) from in situ opposite original electrical-written states in PMN−40%PT. All the images are PFM phase response overlaid on topography. The mechanical force of 2000 nN can induce polarization switching in the vicinity of the 180° c domain wall from c+ to c− or c− to c+ depending on location differences in PMN−32%PT, whereas it induces polarization switching inside the electrical-created c+ domain from c+ to c− in PMN−40%PT.

2.2. Domain Evolution by Mechanical Switching. Evolution of mechanically switched domains under various mechanical loads ranging from 0 to 2000 nN in PMN−32%PT and PMN−40%PT was characterized by PFM. Figure 4a,b illustrates the PFM phase response overlaid on topography in PMN−32%PT on a 3 μm × 3 μm scanning region and in PMN−40%PT on a 1 μm × 1 μm scanning region, respectively. More detailed PFM results of evolution in force can be found in Figure S4 for PMN−32%PT and Figure S5 for PMN−40%PT. Mechanical-induced reversed domains in PMN−32%PT occur in the vicinity of the 180° c domain wall at a load as small as 300 nN, then grow rapidly from 300 to 1400 nN (depicted in Figure S4b–f), and afterward change a little in detail from 1400 to 2000 nN (shown in Figure S4f–l). However, in PMN−40%PT, a mechanical load as large as 1000 nN initiates the occurrence of switched domains which grow then as the loads increase. Similar results of mechanical switching for the other times under various mechanical loads can be found in Figure S6. Notably, the first time mechanical-switched domains (yellow dashed circle in Figure S6a) remain the same during the second time switching process, indicating the stability of the mechanically switched domains. These results indicate that mechanical-induced switching can occur only under a sufficient mechanical load and the onset mechanical load represents the capability of difficulties to be switched by the external field in the materials, analogous to coercive voltage in electrical switching. The smaller onset mechanical force of PMN−32%PT suggests the easier mechanical switching, in comparison to that of PMN−40% PT. On the whole, both of the threshold forces of mechanical switching in the two crystals are low.[27]

Taking the first PFM image after withdrawal of the mechanical force as "0 s", the retention results of the mechanical-induced switched domains in both crystals are depicted in Figures S7–S10. From Figures S7 and S8, the mechanical-induced domains in state 1 do not vanish as time passes by and even grow. Figures S9 and S10 illustrate this time-dependent mechanically switched domain evolution more clearly in PMN−32%PT state 2 and PMN−40%PT, respectively. This time-dependence shown from these results suggests the action of polar nanoregions (PNRs) whose response would have a time delay in the surface.[38,39] According to these domain evolution in time/force, the dynamics and kinetics of the mechanically switched domain motion are analyzed below.

The amplitude changes in mechanical force and time of mechanically switched domain evolution in the two specimens are plotted in Figure 4c,d, respectively. In both cases, the average amplitude of the scanning region decreases first and then increases, with loads or time increasing. The amplitude

DOI: 10.1021/acsami.9b12301
ACS Appl. Mater. Interfaces 2019, 11, 40758−40768

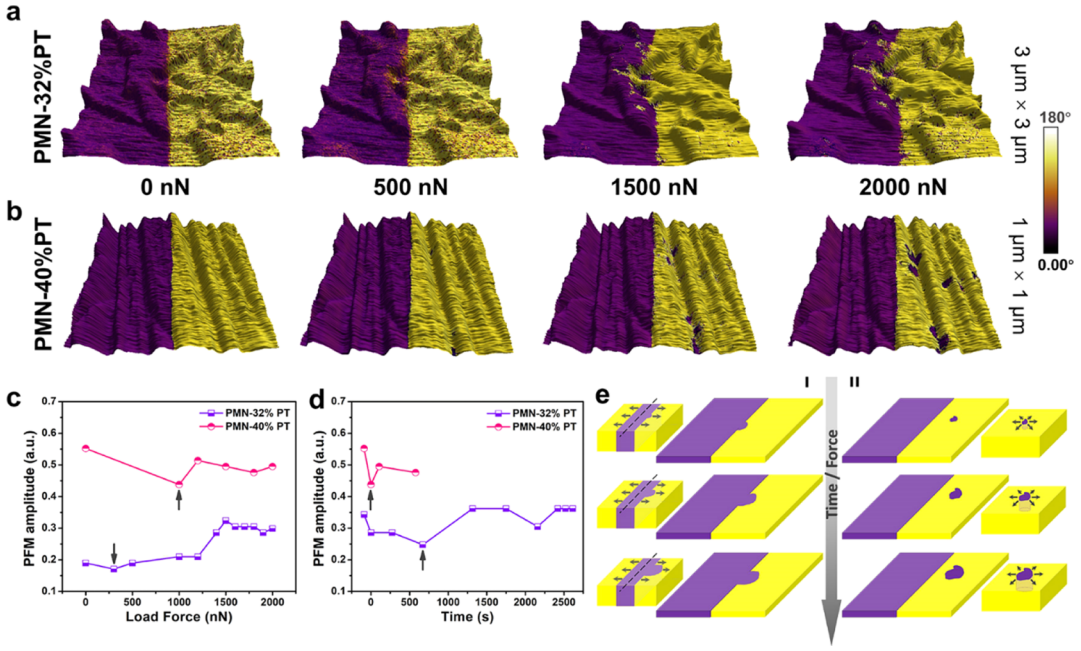

Figure 4. Evolution of mechanically switched domains under various mechanical loads from 0 to 2000 nN in (a) PMN−32%PT on the 3 μm × 3 μm scanning region and (b) PMN−40%PT on the 1 μm × 1 μm scanning region. These images are the PFM phase response overlaid on topography. PFM amplitude changes in (c) mechanical forces and (d) time (after withdrawal of 2000 nN) of mechanically switched domain evolution in PMN−32%PT and PMN−40%PT. The arrows point out the occurrence of the switched domains. (e) Schematics of wall expansion styles and evolution in time/force of the mechanical-reversed domains in (i) PMN−32%PT and (ii) PMN−40%PT.

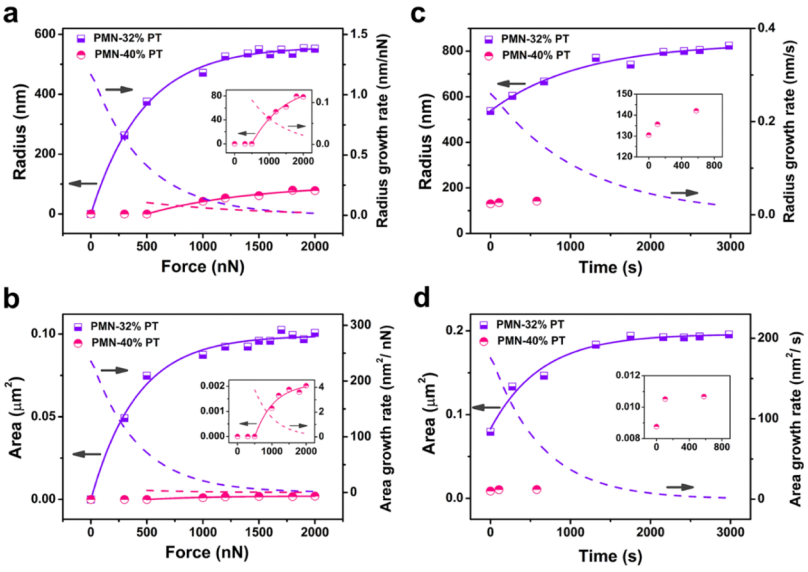

Figure 5. Force-dependence of (a) radius and radius growth rate and (b) area and area growth rate, and time-dependence of (c) radius and radius growth rate and (d) area and area growth rate of the mechanical-switched domains in PMN−32%PT and PMN−40%PT, indicating the metastable and PNR associated property of these induced domains from the point of view of dynamics and kinetics. The scatters show averaged statistical data from the above evolution in time/force results. The solid lines plot the best fitting analysis statistically by equations in the form of $y = a + b \times e^{cx}$ (a, b, c are constants) listed in the main text, exhibiting the exponential growth of the mechanical-induced switched domains in time/force. The dashed lines depict the growth rate. Scatters and lines in purple are for PMN−32%PT and in pink are for PMN−40%PT. The insets show data of PMN−40%PT in an enlarged view.

reaches its smallest value as an indicator of the occurrence of the mechanical-induced domains, similar to that in the electrical-induced polarization switching process by conventional PFM (Figures 1o,p, 2g,h, S1e−h, S4a, and S5a). This trend of amplitude change in force/time is analogous to that with mechanical force increasing, reported in ultrathin $BaTiO_3$ films,[13] which is attributed to the formation of 180° domains with antiparallel polarization.

By nucleating domains which expand afterward, polarization switching proceeds in ferroelectrics commonly.[40] Generally, the domain growth in the polarization switching process includes four stages on the whole, that is, (i) nucleation, (ii) vertical growth, (iii) lateral expansion, and (iv) mergence.

DOI: 10.1021/acsami.9b12301
ACS Appl. Mater. Interfaces 2019, 11, 40758−40768

From the surface changes in our results, three stages except the second one are visualized. Additionally, domain motions can be divided into three conditions according to various dimensions.[41] In the one-dimensional (1-D) condition, domains are flake and their walls move along a single axis. In the two-dimensional (2-D) condition, domains are columnar and their walls expand in the plane perpendicular to the column axis. From the results in Figures S4, S5, S9, and S10, the domain wall in PMN−32%PT (Figures S4 and S9) expands mainly in the direction perpendicular to the 180° c domain wall, satisfying the 1-D condition, whereas that in PMN−40%PT (Figures S5 and S10) expands in the plane parallel to the surface, fitting the 2-D condition. Hence, we can infer that the mechanical-induced domains in PMN−32%PT are flake, obeying the 1-D condition motion behavior, whereas those in PMN−40%PT are columnar and obey the 2-D condition motion behavior. Here, in PMN−40%PT, the switched domains show the same behavior as mentioned in the above mechanical switching for three times, namely, nucleate inside the electrical-created c+ domains and switch into c− nanodomains. In comparison, mechanical switching behaviors are more complex in PMN−32%PT. Whether c+ or c− is more energetically favored under mechanical forces depends on comprehensive factors including local microstructures, homogeneousness, local defects such as oxygen vacancies and so on. Despite these complexities, the mechanical-induced domains are apt to nucleate first in the vicinity of the 180° c domain wall in PMN−32%PT. Considering the differences in nucleation spots and domain expansion styles, the mechanical switching behaviors in the two specimens are divided into two kinds, as illustrated in Figure 4e(i) for PMN−32%PT and Figure 4e(ii) for PMN−40%PT.

Wall velocity limits the speed of switching.[40] Thus, kinetics of switched domains has been investigated roughly.[10] By collecting statistics of the switched domains' area and radius from Figures S4, S5, S9, and S10, the radius and area change in force/time of the mechanically switched domains in PMN−32%PT and PMN−40%PT are plotted in Figure 5. All these results show exponential growth depicted as solid lines and the best statistically fitted equations are listed below. The radius−force plot for PMN−32%PT suits $y = 559.7 - 559.4 \times e^{-0.002130x}$ (Figure 5a in purple solid line) and that for PMN−40%PT fits $y = 100.4 - 170.5 \times e^{-0.001060x}$ (Figure 5a in pink solid line). The area−force plot for PMN−32%PT fits $y = 0.09913 - 0.09913 \times e^{-0.002440x}$ (Figure 5b in purple solid line) and that for PMN−40%PT fits $y = 0.002120 - 0.005250 \times e^{-0.001800x}$ (Figure 5b in pink solid line). For PMN−32%PT, the radius−time plot fits $y = 836.6 - 298.4 \times e^{-8.835x}$ (Figure 5c in purple solid line) and its area−time plot fits $y = 0.5583 - 0.3222 \times e^{-0.0015x}$ (Figure 5d in purple solid line). Then, area and radius growth rates in PMN−32%PT and PMN−40%PT are calculated and plotted as the illustrated dashed lines. Under the same load force, the mechanically switched domain radius in PMN−32%PT is 6−7 times as large as that in PMN−40% PT (Figure 5a) and the domain area in the former is 43−49 times as big as that in PMN−40%PT (Figure 5b). The maximum radius growth rate and area growth rate in PMN−32%PT are 11 times and 30 times as high as those in PMN−40%PT, respectively. Similarly, with time increasing, the switched domain radius, area, and growth rates in PMN−32%PT are much higher than those in PMN−40%PT, as shown in Figure 5c,d. In summary, the same force/time induces switched domains with larger radius and area, together with higher growth rates in PMN−32%PT. Considering these results and the smaller onset force of PMN−32%PT for mechanical switching in comparison to those of PMN−40% PT, it is concluded that the PMN−32%PT is more easily reversed by the mechanical switching process. From these results, generally, after nucleation, the mechanically switched domains in both crystals grow fast at the beginning and then slow down until they reach a stable state. This means that two stages exist during the growth process: (i) metastable stage with rapid growth and (ii) stable stage ultimately.

To differentiate and clarify the effects of mechanical force and time on the domain evolution, in situ switching by various mechanical forces and then aging experiments were performed and the results are illustrated in Figure 6. Intriguingly, time−

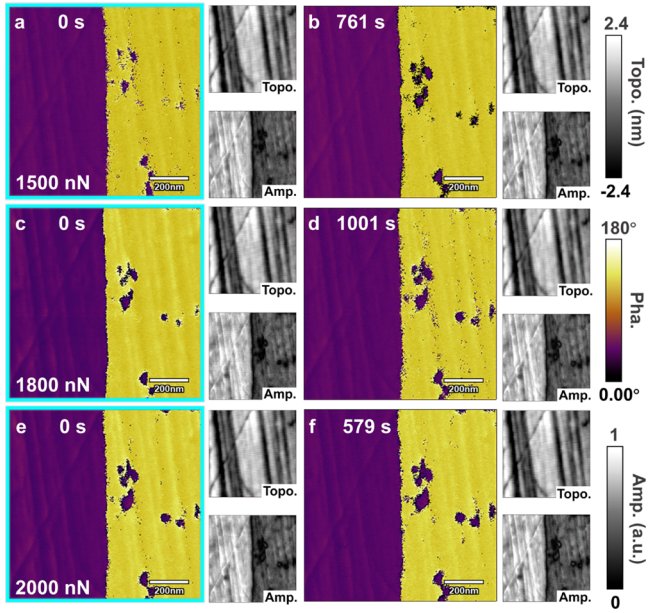

Figure 6. Time−mechanical force equivalence in the mechanical switching, taking PMN−40%PT as an example. The analogous switching behaviors can be acquired by a larger force within a shorter time or a smaller force within a longer time. Take the first PFM image after withdrawal of the mechanical force as "0 s". Domain patterns after mechanical switching by 1500 nN taken at (a) 0 and (b) 761 s. Domain patterns after mechanical switching by 1800 nN taken at (c) 0 and (d) 1001 s. Domain patterns after mechanical switching by 2000 nN taken at (e) 0 and (f) 579 s. PFM phase images are in color, whereas topography and amplitude images are in black and white and labeled with "Topo." and "Amp.", respectively. Mechanical forces were applied to the entire regions enclosed by the cyan squares (1 μm × 1 μm).

mechanical force equivalence is visualized here, similar to the well-known time−temperature equivalence principle in mechanical relaxation in polymers. The analogous switching behaviors can be acquired by a larger force within a shorter time or a smaller force within a longer time, as long as the forces are larger than the onset force for mechanical switching.

2.3. Mechanism Discussion. Piezoelectricity and flexoelectricity are broadly visualized in ferroelectric oxides and generally, the former is stronger than the latter.[13] The pure mechanical pressure-induced piezoelectric effect can only rotate polarization orientation from vertical to lateral, that is, from c domains to a domains (polarization of whose are in-plane).[17] However, the domains observed here are all c

DOI: 10.1021/acsami.9b12301
ACS Appl. Mater. Interfaces 2019, 11, 40758−40768

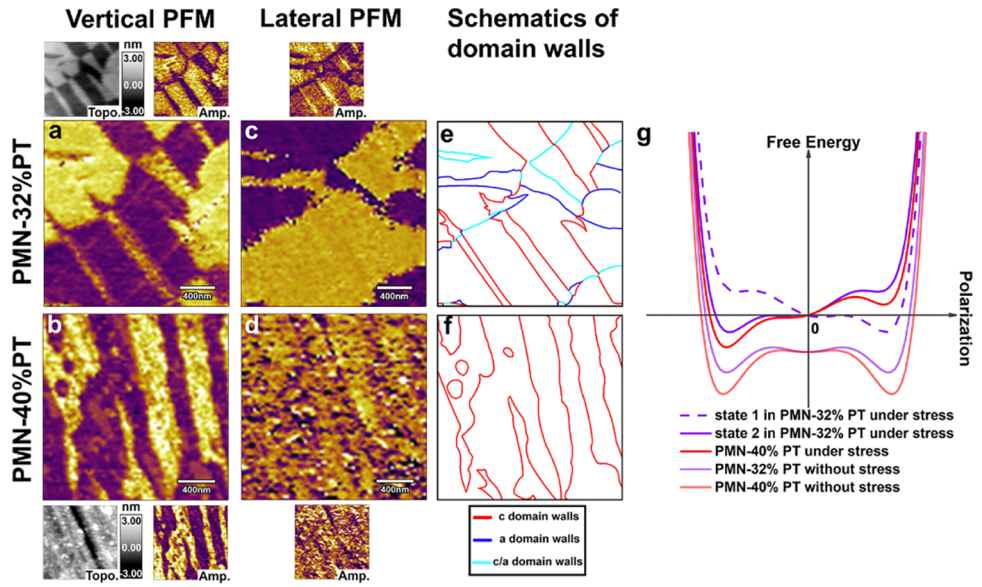

Figure 7. Vertical and lateral domain configurations in PMN−32%PT and PMN−40%PT by vector PFM: (a) vertical and (c) lateral PFM phase signals in PMN−32%PT; (b) vertical and (d) lateral phase signals in PMN−40%PT. Schematics of corresponding domain walls in (e) PMN−32% PT and (f) PMN−40%PT. (g) Schematics of free energy versus polarization in PMN−32%PT and PMN−40%PT under/without stress. Topography and amplitude images are presented above/below their corresponding phase images, labeled with "Topo." and "Amp.", respectively.

domains; thus, the mechanical-induced switching cannot be ascribed to the bulk piezoelectric effect.

Except in thin films as mentioned in the introduction, flexoelectricity exists in dielectric solids as well. The flexoelectric coefficients of most dielectric solids, especially the simple ones, are estimated theoretically to be too small[34,42,43] to induce sufficient strain gradient for mechanical switching. Particularly, flexoelectricity can be omitted when other electromechanical responses (e.g., piezoelectricity) exist in the materials.[39,44] However, it was later found that in some dielectrics owning to high permittivity, their flexoelectricity is unexpectedly largely enhanced and possibly sufficient to induce polarization,[34,43] where the flexoelectric coefficients are in several or even tens of orders of higher magnitude.[43−47] These reported high permittivity dielectrics with giant flexoelectricity include paraelectric $SrTiO_3$,[48] and perovskite piezoelectrics, especially perovskite relaxors such as PMN,[47,49] perovskite ferroelectrics such as Pb-based systems like $Pb(Zr,Ti)O_3$,[46,50] $BaTiO_3$-based systems like $BaTiO_3$,[51,52] $Ba(Ti,Sn)O_3$,[53] $BaTiO_3$−$Ba(Zr,Ti)O_3$,[54] and $(K,Na)NbO_3$-based systems,[55] and perovskite relaxor ferroelectrics like PMN−PT[39,43,56−58] and PIN−PMN−PT.[44] According to Tagantsev's flexoelectric theory,[59,60] the possible mechanisms of these enhanced flexoelectricity in bulks include four contributions: dynamic bulk flexoelectricity, static bulk flexoelectricity, surface flexoelectricity, and surface piezoelectricity.[52,61] The mechanisms of a barrier layer,[61] inner microstrains resulted from macroscopic centric symmetry breaking,[62] ferroelectricity,[44,55] and PNRs[39,43] are also proposed recently. In relaxor ferroelectrics such as PMN−PT, PIN−PMN−PT single crystal, it is believed that polar nanodomain rotation polarization,[39,43] residual piezoelectricity,[45] surface piezoelectricity,[45] and surface flexoelectricity[57] can give rise to these enhanced flexoelectric behaviors. Notably, the PNRs are reported to be one important source of the residual flexoelectricity.[43,45] Besides, PNRs are in dominant contribution (50−80%) to the room-temperature ultrahigh piezoelectricity in relaxor ferroelectric solid solution crystals,[56] which can facilitate polarization rotation and enhance ferroelectricity/piezoelectricity and thus couple extrinsically[44,55] with their flexoelectricity. All of these indicate the probable dominant role of PNRs in generating the enhanced flexoelectricity in relaxor ferroelectric crystals. Intriguingly, in the surface, the response of PNRs would have a time delay,[39] which can account for the time-dependence of mechanical switching observed in this work.

The chemical makeup, structure, and existence of PNRs of PMN−PT bulks determine their exhibiting the reported huge flexoelectric coefficients[45] which suggest the significant role of flexoelectricity in affecting the polarization. Besides, our crystals are 200 μm thick and comparable to a thick film. The application of electric voltage/mechanical force from the SPM tip to the sample surface could only impact upon the top surface region, the depth of which is quite difficult to be determined exactly or directly, owing to the heterogeneous field under the tip.[13,20,34,40,63] The depth of this electric or mechanical potential under the biased tip has a relationship with the radius of the tip, the tip-surface contact area, and many other parameters.[13,40,63] Whether the domains are reversed throughout the thickness direction primarily depends on the magnitude of the electric/flexoelectric field. In general, the electrically polarized bipolar domains in the crystals exist in the surface layer possibly in a thickness of dozens of nanometers, and the mechanically induced domains may exist in the top surface of the electrical-created surface layer. The latter can be considered as a "skin structure" (in a typical depth of $\lesssim$1 μm) where internal chemical pressure induced by action of oxygen vacancies and surface plane stress combine to specialize its properties.[64] This skin, whose driving force of formation is calculated to be provided by oxygen vacancies,[64] is reported to influence the flexoelectric effect. Moreover, the force by the AFM tip can induce a large flexoelectric field[42,65] in this abovementioned "skin structure", which would be sufficient to generate local polarization rotation.[13] By rough estimation of the tip-surface contact area as a disk of 10 nm[13] in radius, the 750 nN of force over the contact area is

DOI: 10.1021/acsami.9b12301
ACS Appl. Mater. Interfaces 2019, 11, 40758−40768

equivalent to a compressive uniaxial stress of ∼2.4 GPa. Similarly, the 1200 nN induces a stress of ∼3.8 GPa in the 80 nm-thick film. On the same estimation, the 2000 nN causes a pressure of ∼6.4 GPa in our experiments. In addition, the surface piezoelectricity depends on the local symmetry, surface permittivity, and surface conditions[49] and thus accounts for similar but different mechanical switching states in PMN−32% PT. Last but not the least, defects such as oxygen vacancies,[20] vacancy dipoles, and clusters exist in the ferroelectric single crystals, especially in the top surface, serving as nucleation sites for polarization switching and pinning sites for domain wall motion.[66] These vacancies, being elastic dipoles, can affect the electric fields and polarization through bulk Vegard strain effect,[20,21,63,67] and flexoelectricity,[67] which will contribute to the mechanical switching as well.

From another aspect, the switching existence layer can be simplified and considered as a thin film due to its thin thickness (nanometers, in comparison with that of the whole sample on the scale of hundreds of micrometers) and thus explanations for mechanical switching in thin films mentioned in the introduction can be taken into consideration.

In PMN−40%PT, the tip-induced pressure leads to a switching from original c+ domain to c− nanodomains, whereas the original c− domain does not respond to the mechanical force at all. This phenomenon is analogous to that reported in 80 nm-thick c-oriented $PbTiO_3$ films,[25] and can be ascribed to asymmetric interaction between the domain structures and the strain gradient via flexoelectric effect. With regard to PMN−32%PT, mechanical switching generally occurs in the vicinity of the 180° domain wall, and the switch of c+ or c− depends locally on the selected regions. The origins of flexoelectricity in this specimen are more complex. Strong coupling in between polarization rotation and lattice strain exists in its monoclinic phase,[35] and is supported further by the experimental results of the unique mechanical switching occurrence around the 180° domain wall. This behavior can be ascribed to the orderslower magnitude of nucleation bias at the 180° domain wall compared with that required for domain nucleation in the bulk.[37] Moreover, a/c domain walls exist in PMN−32%PT but not in PMN−40%PT, as illustrated in Figure 7a−f. Local stress gradients exist near these a/c twin walls and thus create lateral and vertical electric fields via the flexoelectric effect, resulting in polarization rotation. Similar findings are reported in $BaTiO_3$ ultrathin films by experiments[13] and in $PbZr_{1-x}Ti_xO_3$ thin films by phase-field simulation.[22] In addition, considering the free energy, a polar bias is generated by the inhomogeneous strain gradient[13] resulted from flexoelectricity, as illustrated in Figure 7g. In PMN−40%PT with tetragonal symmetry, this bias destabilizes the c+ domains of the double well and thus forces the reversal to c− domains.[13] In contrast, in PMN−32%PT with monoclinic symmetry, the destabilization by the polar bias of c+ or c− domains has a close relationship with the local regions where original domain structures and surface conditions affect a lot,[10] and thus two states exist depending on certain circumstances. However, overall, the energy barrier of mechanical switching in PMN−32%PT is lower than that in PMN−40%PT; thus, the former has a smaller onset mechanical load. Finally, oxygen vacancies influence the flexoelectricity via Vegard strain effect as well.

The strain gradient induced by a force of 2000 nN from the tip is sufficient to induce local switching partially from the electrically polarized bipolar domains on the crystals surface, nevertheless, it is insufficient to reverse the pristine domains in the crystals directly. In comparison, these pristine domains can be totally reversed by electric voltage with a magnitude of 20 V. We believe that the flexoelectric field induced by the force of 2000 nN is larger than the mechanical switching threshold of domains in the electrical-switched thin layers of the two specimens; thus, nucleation and growth of the switching can be initiated. However, this field is insufficient to reverse the domains completely down to the bottom of the thin layer, not to mention through the whole thickness of the crystals. Notably, mechanical loading forces are reported to have equivalent effects on the polarization switching as the electric voltages. For instance, an applied force of 750 nN leads to equivalent switching in $BaTiO_3$ ultrathin films at an application of 1.25 V;[13] a force of 1050 nN equals a dc electric voltage of 3 V on the switching in $PbZr_{0.2}Ti_{0.8}O_3$ films;[27] and a loading force of 1200 nN causes similar switching in 80 nm-thick $PbTiO_3$ films as a 2.1 V dc bias does.[25] Considering the equivalence of electric and mechanical bias, we deduce that the mechanical switching would be through the depth under sufficiently large forces. Meanwhile, these results indicate that pre-electrical writing may be a possible good supplementary way to help induce sufficient strain gradient in bulks during mechanical switching.

To sum up, in our experiments, electrical switching leads to polarization reversal, creating bipolar c domains in a thin layer on the surface of the crystals first. Then, these domains are switched by mechanical forces through a strain-gradient-induced flexoelectric field. This field is coupled with polarization switching. Flexoelectricity and Vegard strain effect originated from surface oxygen vacancies are the dominant mechanisms of these visualized mechanical switching behaviors. Surface piezoelectricity accounts for the behaviors as well. The origins of the flexoelectricity in the two crystals are different: asymmetric interaction between the domain structures and the strain gradient in PMN−40%PT, and a comprehensive and complex effect due to strong coupling in the monoclinic phase and lateral and vertical electric fields stemmed from local stress gradients near its a/c twin domain walls in PMN−32%PT. PNRs are responsible for the time-dependent mechanical switching behaviors in both crystals and surface piezoelectricity accounts for the analogous but different switching states in PMN−32%PT.

3. CONCLUSIONS

Mechanical-induced polarization switching in relaxor ferroelectric $(1 - x\%)Pb(Mg_{1/3}Nb_{2/3})O_3-x\%PbTiO_3$ (PMN−x% PT, x = 32, 40) single crystals was investigated via SPM. Mechanical forces larger than the low onset load induce metastable and electrically erasable domain reversal and wall motion from electrical-created bipolar domains in both crystals. Detailed studies on switching dynamics and kinetics suggest the local symmetry dependence of the diverse mechanical switching behaviors, especially in nucleation sites, expansion paths, and growth rates. This work further demonstrates force- and time-dependence, time-force equivalence of the mechanical switching. The time-dependent mechanical switching behavior reveals the action and contribution of PNRs. Flexoelectricity and bulk Vegard strain effect give rise to these mechanical switching behaviors. These investigations help deepen the understanding of domains in relaxor ferroelectrics, and provide opportunities in manipulat-

DOI: 10.1021/acsami.9b12301
ACS Appl. Mater. Interfaces 2019, 11, 40758−40768

ing domain patterns physically in crystals by various switching methods for domain engineering and device making.

4. METHODS AND MATERIALS

4.1. Sample Preparation. Commercial (100)-oriented unpoled relaxor ferroelectric $(1 - x\%)Pb(Mg_{1/3}Nb_{2/3})O_3-x\%PbTiO_3$ (PMN−x%PT) (x = 32, 40) single crystals (MTI Group, Hefei) were chosen as study objects because of their easy accessibility and definite correspondence between compositions and symmetry structures: monoclinic (M) symmetry in the PMN−32%PT and tetragonal (T) symmetry for the PMN−40%PT. These specimens are in a size of 5 mm × 5 mm × 0.2 mm and polished to an optical surface finish.

4.2. Scanning Probe Microscopy. A multifunctional SPM (Cypher S, Asylum Research, USA) combined with AFM and PFM and other PFM-derived modes such as litho PFM and vector PFM was utilized in our experiments. Conductive Ti/Pt-coated silicon cantilevers (AC240TM-R3, Olympus) with spring constant of ∼2 N m^{-1} and labeled radius of 28 ± 10 nm were used in all modes. In this work, the spring constant of the chosen tip determined the largest applied force in the value of ∼2000 nN. Thermal drift may result from thermal disequilibrium of the system, slow scan rate, and long-time scanning. To minimize this effect, 2 h were taken before measurements for the whole system to reach its thermal equilibrium. The scan rates of PFM scanning and switching were set at 3.91 and 1 Hz, respectively, both of which are sufficiently fast. For in situ and retention characterizations, the scanning regions were fine-tuned during the whole test using a special feature, that is, the central 180° domain wall, as a reference in the image to track the thermal drift and ensure the same scanning regions. Fine-tuning the scanning region would not change the testing parameters, but affect the imaging collection interval time. Therefore, thermal drift should not have a significant influence on the results of PFM in situ characterization. However, for the presented in situ domain evolution results, retention images were taken under varied interval times. Owing to the high phase transition temperature of these samples, thermal fluctuation only induces thermal shift but has no effect on the sample ferroelectric properties and our PFM data.

4.3. Topography and Domain Configuration Characterization. PFM mode was taken to image the pristine state over 7 μm × 7 μm and switching-after ferroelectric domain configurations with out-of-plane polarization (c domains) in the specimens, with a 0.8 V (equivalent to ∼100 nN) ac voltage at a resonant frequency of 260 kHz applied to the tip. Both the vertical and lateral PFM domain structures in the single crystals were characterized through vector PFM.

4.4. Statistical Analyses of Domain Radius and Area. Domains can be identified combining the PFM amplitude and phase responses together. Domains with opposite polarization directions show different color contrast in the PFM phase images (e.g., purple and yellow), separated by boundaries whose PFM amplitudes are the lowest (in the presence of black lines in general) from the black and white PFM amplitude images. The switched domains can thus be identified. In this work, all the mechanical-induced switched domains in the two specimens are not typically round, but rather in a convex shape. In mathematics, the diameter of a convex pattern is defined as the longest distance of the attachment between any two points. The area is defined as the region taken over. The radius and area were calculated by the software ImageJ using the function named "Measure", via "Straight line selections" and "Freehand selections", respectively. An average value was calculated based on 15−20 measurements for each domain. The radius/area range was given in the paper by statistical analyses of these average data.

4.5. Electrical Switching Measurements. Electrical-created bipolar domains were written locally on the central 5 μm × 5 μm regions from their pristine state domains in the two single crystals by litho PFM, applying external dc electric voltages with a magnitude of 20 V (larger than coercive voltage). On the left half side, a dc voltage of +20 V induces the c− domain with polarization downward, whereas on the right side, a dc voltage of -20 V leads to the c+ domain with polarization upward. In both the first and second electrical erasure processes, dc electric voltages with a magnitude of 20 V were applied by certain patterns via litho PFM over the central 1 μm × 1 μm region. For the first time erasure, dc voltages of + 20 and −20 V were applied on the left and right half sides, respectively, whereas for the second time erasure, a dc voltage of −20 V was applied on the left and +20 V on the right.

4.6. Mechanical Switching Measurements. In the mechanical switching process, mechanical loads of 300−2000 nN from the tip were applied to pristine state c domains first and then to electrical-created bipolar domains during scanning all over the selected regions by AFM in contact mode, after calibrating parameters of the cantilever. Forces were applied over the central 3 μm × 3 μm, 1 μm × 1 μm, and 1 μm × 1 μm regions from the electrical-created bipolar domains for the first, second, and third times, respectively. The mechanical scanning direction is perpendicular to the electrical-created bipolar c domain walls.

4.7. Retention and Kinetics Measurements. In the aging experiments, PFM was utilized to characterize the mechanical-induced domain evolution in time after mechanical switching. The software ImageJ was used for the statistical analysis of domain kinetics, such as area and radius growth of the mechanical-switched domains.

■ ASSOCIATED CONTENT

Supporting Information

The Supporting Information is available free of charge on the ACS Publications website at DOI: 10.1021/acsami.9b12301.

Additional PFM response images (topography, amplitude, and phase) of domain patterns created by mechanical loading or electrical poling for three times, domain evolution under various mechanical loads, and in situ domain retention indicating time-dependent domain evolution in the PMN−32%PT and PMN−40%PT single crystals (PDF)

■ AUTHOR INFORMATION

Corresponding Author

*E-mail: yaodongy@xjtu.edu.cn.

ORCID

Yaodong Yang: 0000-0002-1707-0633

Notes

The authors declare no competing financial interest.

■ ACKNOWLEDGMENTS

This work was supported by the National Key R&D Program of China (2017YFA0208000), the National Science Foundation of China (Grant Nos. 51831010, 51621063), the Program for Changjiang Scholars and Innovative Research Team in University (IRT_17R85), and the Fundamental Research Funds for the Central Universities (xtr0118016).

■ REFERENCES

(1) Gruverman, A.; Wu, D.; Scott, J. F. Piezoresponse Force Microscopy Studies of Switching Behavior of Ferroelectric Capacitors on a 100-ns Time Scale. *Phys. Rev. Lett.* **2008**, *100*, 097601.

(2) Kalinin, S. V.; Morozovska, A. N.; Chen, L. Q.; Rodriguez, B. J. Local Polarization Dynamics in Ferroelectric Materials. *Rep. Prog. Phys.* **2010**, *73*, 056502.

(3) Ievlev, A. V.; Brown, C. C.; Agar, J. C.; Velarde, G. A.; Martin, L. W.; Belianinov, A.; Maksymovych, P.; Kalinin, S. V.; Ovchinnikova, O. S. Nanoscale Electrochemical Phenomena of Polarization Switching in Ferroelectrics. *ACS Appl. Mater. Interfaces* **2018**, *10*, 38217−38222.

DOI: 10.1021/acsami.9b12301
ACS Appl. Mater. Interfaces 2019, 11, 40758−40768

(4) Chen, D.; Chen, Z.; He, Q.; Clarkson, J. D.; Serrao, C. R.; Yadav, A. K.; Nowakowski, M. E.; Fan, Z.; You, L.; Gao, X.; Zeng, D.; Chen, L.; Borisevich, A. Y.; Salahuddin, S.; Liu, J.-M.; Bokor, J. Interface Engineering of Domain Structures in $BiFeO_3$ Thin Films. *Nano Lett.* **2017**, *17*, 486−493.
(5) Chen, D.; Gao, X.; Liu, J.-M. Domain Structures and Magnetoelectric Effects in Multiferroic Nanostructures. *MRS Commun.* **2016**, *6*, 330−340.
(6) Jesse, S.; Rodriguez, B. J.; Choudhury, S.; Baddorf, A. P.; Vrejoiu, I.; Hesse, D.; Alexe, M.; Eliseev, E. A.; Morozovska, A. N.; Zhang, J.; Chen, L.-Q.; Kalinin, S. V. Direct Imaging of the Spatial and Energy Distribution of Nucleation Centres in Ferroelectric Materials. *Nat. Mater.* **2008**, *7*, 209−215.
(7) Agar, J. C.; Cao, Y.; Naul, B.; Pandya, S.; van der Walt, S.; Luo, A. I.; Maher, J. T.; Balke, N.; Jesse, S.; Kalinin, S. V.; Vasudevan, R. K.; Martin, L. W. Machine Detection of Enhanced Electromechanical Energy Conversion in $PbZr_{0.2}Ti_{0.8}O_3$ Thin Films. *Adv. Mater.* **2018**, *30*, 1800701.
(8) Rodriguez, B. J.; Jesse, S.; Alexe, M.; Kalinin, S. V. Spatially Resolved Mapping of Polarization Switching Behavior in Nanoscale Ferroelectrics. *Adv. Mater.* **2008**, *20*, 109−114.
(9) Kalinin, S. V.; Kim, Y.; Fong, D. D.; Morozovska, A. N. Surface-Screening Mechanisms in Ferroelectric Thin Films and Their Effect on Polarization Dynamics and Domain Structures. *Rep. Prog. Phys.* **2018**, *81*, 036502.
(10) Gao, P.; Britson, J.; Nelson, C. T.; Jokisaari, J. R.; Duan, C.; Trassin, M.; Baek, S. H.; Guo, H.; Li, L.; Wang, Y.; Chu, Y. H.; Minor, A. M.; Eom, C. B.; Ramesh, R.; Chen, L. Q.; Pan, X. Ferroelastic Domain Switching Dynamics under Electrical and Mechanical Excitations. *Nat. Commun.* **2014**, *5*, 3801.
(11) Chu, K.; Jang, B.-K.; Sung, J. H.; Shin, Y. A.; Lee, E.-S.; Song, K.; Lee, J. H.; Woo, C.-S.; Kim, S. J.; Choi, S.-Y.; Koo, T. Y.; Kim, Y.-H.; Oh, S.-H.; Jo, M.-H.; Yang, C.-H. Enhancement of the Anisotropic Photocurrent in Ferroelectric Oxides by Strain Gradients. *Nat. Nanotechnol.* **2015**, *10*, 972−979.
(12) Balke, N.; Choudhury, S.; Jesse, S.; Huijben, M.; Chu, Y. H.; Baddorf, A. P.; Chen, L. Q.; Ramesh, R.; Kalinin, S. V. Deterministic Control of Ferroelastic Switching in Multiferroic Materials. *Nat. Nanotechnol.* **2009**, *4*, 868−875.
(13) Lu, H.; Bark, C.-W.; Esque de los Ojos, D.; Alcala, J.; Eom, C. B.; Catalan, G.; Gruverman, A. Mechanical Writing of Ferroelectric Polarization. *Science* **2012**, *336*, 59−61.
(14) Zhang, Q.; Prokhorenko, S.; Nahas, Y.; Xie, L.; Bellaiche, L.; Gruverman, A.; Valanoor, N. Deterministic Switching of Ferroelectric Bubble Nanodomains. *Adv. Funct. Mater.* **2019**, *29*, 1808573.
(15) Damodaran, A. R.; Pandya, S.; Agar, J. C.; Cao, Y.; Vasudevan, R. K.; Xu, R.; Saremi, S.; Li, Q.; Kim, J.; McCarter, M. R.; Dedon, L. R.; Angsten, T.; Balke, N.; Jesse, S.; Asta, M.; Kalinin, S. V.; Martin, L. W. Three-State Ferroelastic Switching and Large Electromechanical Responses in $PbTiO_3$ Thin Films. *Adv. Mater.* **2017**, *29*, 1702069.
(16) Jeon, B. C.; Lee, D.; Lee, M. H.; Yang, S. M.; Chae, S. C.; Song, T. K.; Bu, S. D.; Chung, J.-S.; Yoon, J.-G.; Noh, T. W. Flexoelectric Effect in the Reversal of Self-Polarization and Associated Changes in the Electronic Functional Properties of $BiFeO_3$ Thin Films. *Adv. Mater.* **2013**, *25*, 5643−5649.
(17) Cao, Y.; Morozovska, A. N.; Kalinin, S. V. Pressure-Induced Switching in Ferroelectrics: Phase-Field Modeling, Electrochemistry, Flexoelectric Effect, and Bulk Vacancy Dynamics. *Phys. Rev. B* **2017**, *96*, 184109.
(18) Park, S. M.; Wang, B.; Das, S.; Chae, S. C.; Chung, J.-S.; Yoon, J.-G.; Chen, L.-Q.; Yang, S. M.; Noh, T. W. Selective Control of Multiple Ferroelectric Switching Pathways Using a Trailing Flexoelectric Field. *Nat. Nanotechnol.* **2018**, *13*, 366−370.
(19) Vorotiahin, I. S.; Eliseev, E. A.; Li, Q.; Kalinin, S. V.; Genenko, Y. A.; Morozovska, A. N. Tuning the Polar States of Ferroelectric Films via Surface Charges and Flexoelectricity. *Acta Mater.* **2017**, *137*, 85−92.
(20) Das, S.; Wang, B.; Cao, Y.; Rae Cho, M.; Jae Shin, Y.; Mo Yang, S.; Wang, L.; Kim, M.; Kalinin, S. V.; Chen, L. Q.; Noh, T. W. Controlled Manipulation of Oxygen Vacancies Using Nanoscale Flexoelectricity. *Nat. Commun.* **2017**, *8*, 615.
(21) Glinchuk, M. D.; Eliseev, E. A.; Li, G. R.; Zeng, J. T.; Kalinin, S. V.; Morozovska, A. N. Ferroelectricity Induced by Oxygen Vacancies in Relaxors with Perovskite Structure. *Phys. Rev. B* **2018**, *98*, 094102.
(22) Cao, Y.; Chen, L.-Q.; Kalinin, S. V. Role of Flexoelectric Coupling in Polarization Rotations at the a-c Domain Walls in Ferroelectric Perovskites. *Appl. Phys. Lett.* **2017**, *110*, 202903.
(23) Jablonski, M. L.; Liu, S.; Winkler, C. R.; Damodaran, A. R.; Grinberg, I.; Martin, L. W.; Rappe, A. M.; Taheri, M. L. Asymmetric Response of Ferroelastic Domain-Wall Motion under Applied Bias. *ACS Appl. Mater. Interfaces* **2016**, *8*, 2935−2941.
(24) Wang, Y.-J.; Zhu, Y.-L.; Ma, X.-L. Chiral Phase Transition at 180° Domain Walls in Ferroelectric $PbTiO_3$ Driven by Epitaxial Compressive Strains. *J. Appl. Phys.* **2017**, *122*, 134104.
(25) Lu, H.; Liu, S.; Ye, Z.; Yasui, S.; Funakubo, H.; Rappe, A. M.; Gruverman, A. Asymmetry in Mechanical Polarization Switching. *Appl. Phys. Lett.* **2017**, *110*, 222903.
(26) Catalan, G.; Lubk, A.; Vlooswijk, A. H. G.; Snoeck, E.; Magen, C.; Janssens, A.; Rispens, G.; Rijnders, G.; Blank, D. H. A.; Noheda, B. Flexoelectric Rotation of Polarization in Ferroelectric Thin Films. *Nat. Mater.* **2011**, *10*, 963.
(27) Guo, E. J.; Roth, R.; Das, S.; Dörr, K. Strain Induced Low Mechanical Switching Force in Ultrathin $PbZr_{0.2}Ti_{0.8}O_3$ Films. *Appl. Phys. Lett.* **2014**, *105*, 012903.
(28) Alsubaie, A.; Sharma, P.; Lee, J. H.; Kim, J. Y.; Yang, C.-H.; Seidel, J. Uniaxial Strain-Controlled Ferroelastic Domain Evolution in $BiFeO_3$. *ACS Appl. Mater. Interfaces* **2018**, *10*, 11768−11775.
(29) Li, Y.-J.; Wang, J.-J.; Ye, J.-C.; Ke, X.-X.; Gou, G.-Y.; Wei, Y.; Xue, F.; Wang, J.; Wang, C.-S.; Peng, R.-C.; Deng, X.-L.; Yang, Y.; Ren, X.-B.; Chen, L.-Q.; Nan, C.-W.; Zhang, J.-X. Mechanical Switching of Nanoscale Multiferroic Phase Boundaries. *Adv. Funct. Mater.* **2015**, *25*, 3405−3413.
(30) Zhao, X.-W.; Dong, S.-N.; Gao, G.-Y.; Xu, Z.-X.; Xu, M.; Yan, J.-M.; Zhao, W.-Y.; Liu, Y.-K.; Yan, S.-Y.; Zhang, J.-X.; Wang, Y.; Lu, H.-Z.; Li, X.-G.; Furdyna, J. K.; Luo, H.-S.; Zheng, R.-K. Reversible and Nonvolatile Manipulation of the Electronic Transport Properties of Topological Insulators by Ferroelectric Polarization Switching. *npj Quantum Mater.* **2018**, *3*, 52.
(31) Davis, M. Picturing the Elephant: Giant Piezoelectric Activity and the Monoclinic Phases of Relaxor-Ferroelectric Single Crystals. *J. Electroceram.* **2007**, *19*, 25−47.
(32) Krogstad, M. J.; Gehring, P. M.; Rosenkranz, S.; Osborn, R.; Ye, F.; Liu, Y.; Ruff, J. P. C.; Chen, W.; Wozniak, J. M.; Luo, H.; Chmaissem, O.; Ye, Z.-G.; Phelan, D. The Relation of Local Order to Material Properties in Relaxor Ferroelectrics. *Nat. Mater.* **2018**, *17*, 718−724.
(33) Liu, M.; Hoffman, J.; Wang, J.; Zhang, J.; Nelson-Cheeseman, B.; Bhattacharya, A. Non-Volatile Ferroelastic Switching of the Verwey Transition and Resistivity of Epitaxial Fe_3O_4/PMN-PT (011). *Sci. Rep.* **2013**, *3*, 1876.
(34) Zubko, P.; Catalan, G.; Tagantsev, A. K. Flexoelectric Effect in Solids. *Annu. Rev. Mater. Res.* **2013**, *43*, 387−421.
(35) Liu, H.; Chen, J.; Fan, L.; Ren, Y.; Hu, L.; Guo, F.; Deng, J.; Xing, X. Structural Evidence for Strong Coupling between Polarization Rotation and Lattice Strain in Monoclinic Relaxor Ferroelectrics. *Chem. Mater.* **2017**, *29*, 5767−5771.
(36) Shvartsman, V. V.; Dkhil, B.; Kholkin, A. L. Mesoscale Domains and Nature of the Relaxor State by Piezoresponse Force Microscopy. *Annu. Rev. Mater. Res.* **2013**, *43*, 423−449.
(37) Aravind, V. R.; Morozovska, A. N.; Bhattacharyya, S.; Lee, D.; Jesse, S.; Grinberg, I.; Li, Y. L.; Choudhury, S.; Wu, P.; Seal, K.; Rappe, A. M.; Svechnikov, S. V.; Eliseev, E. A.; Phillpot, S. R.; Chen, L. Q.; Gopalan, V.; Kalinin, S. V. Correlated Polarization Switching in the Proximity of a 180° Domain Wall. *Phys. Rev. B: Condens. Matter Mater. Phys.* **2010**, *82*, 024111.
(38) Kalinin, S. V.; Rodriguez, B. J.; Budai, J. D.; Jesse, S.; Morozovska, A. N.; Bokov, A. A.; Ye, Z. G. Direct Evidence of Mesoscopic Dynamic Heterogeneities at the Surfaces of Ergodic

DOI: 10.1021/acsami.9b12301
ACS Appl. Mater. Interfaces 2019, 11, 40758−40768

Ferroelectric Relaxors. *Phys. Rev. B: Condens. Matter Mater. Phys.* **2010**, *81*, 064107.
(39) Shu, L.; Wan, M.; Jiang, X.; Li, F.; Zhou, N.; Huang, W.; Wang, T. Frequency Dispersion of Flexoelectricity in PMN-PT Single Crystal. *AIP Adv.* **2017**, *7*, 015010.
(40) Guo, E.-J.; Roth, R.; Herklotz, A.; Hesse, D.; Dörr, K. Ferroelectric 180 Degrees Domain Wall Motion Controlled by Biaxial Strain. *Adv. Mater.* **2015**, *27*, 1615−1618.
(41) Ishibashi, Y.; Takagi, Y. Note on Ferroelectric Domain Switching. *J. Phys. Soc. Jpn.* **1971**, *31*, 506−510.
(42) Nguyen, T. D.; Mao, S.; Yeh, Y.-W.; Purohit, P. K.; McAlpine, M. C. Nanoscale Flexoelectricity. *Adv. Mater.* **2013**, *25*, 946−974.
(43) Narvaez, J.; Catalan, G. Origin of The Enhanced Flexoelectricity of Relaxor Ferroelectrics. *Appl. Phys. Lett.* **2014**, *104*, 162903.
(44) Shu, L.; Li, T.; Wang, Z.; Li, F.; Fei, L.; Rao, Z.; Ye, M.; Ke, S.; Huang, W.; Wang, Y.; Yao, X. Flexoelectric Behavior in PIN-PMN-PT Single Crystals over a Wide Temperature Range. *Appl. Phys. Lett.* **2017**, *111*, 162901.
(45) Huang, S.; Qi, L.; Huang, W.; Shu, L.; Zhou, S.; Jiang, X. Flexoelectricity in Dielectrics: Materials, Structures and Characterizations. *J. Adv. Dielectr.* **2018**, *08*, 1830002.
(46) Ma, W.; Cross, L. E. Flexoelectric Effect in Ceramic Lead Zirconate Titanate. *Appl. Phys. Lett.* **2005**, *86*, 072905.
(47) Ma, W.; Cross, L. E. Observation of the Flexoelectric Effect in Relaxor $Pb(Mg_{1/3}Nb_{2/3})O_3$ Ceramics. *Appl. Phys. Lett.* **2001**, *78*, 2920−2921.
(48) Zubko, P.; Catalan, G.; Buckley, A.; Welche, P. R.; Scott, J. F. Strain-Gradient-Induced Polarization in $SrTiO_3$ Single Crystals. *Phys. Rev. Lett.* **2007**, *99*, 167601.
(49) Ma, W.; Cross, L. E. Large Flexoelectric Polarization in Ceramic Lead Magnesium Niobate. *Appl. Phys. Lett.* **2001**, *79*, 4420−4422.
(50) Ma, W.; Cross, L. E. Strain-Gradient-Induced Electric Polarization in Lead Zirconate Titanate Ceramics. *Appl. Phys. Lett.* **2003**, *82*, 3293−3295.
(51) Ma, W.; Cross, L. E. Flexoelectricity of Barium Titanate. *Appl. Phys. Lett.* **2006**, *88*, 232902.
(52) Narvaez, J.; Saremi, S.; Hong, J.; Stengel, M.; Catalan, G. Large Flexoelectric Anisotropy in Paraelectric Barium Titanate. *Phys. Rev. Lett.* **2015**, *115*, 037601.
(53) Shu, L.; Wan, M.; Wang, Z.; Wang, L.; Lei, S.; Wang, T.; Huang, W.; Zhou, N.; Wang, Y. Large Flexoelectricity in Al_2O_3-doped $Ba(Ti_{0.85}Sn_{0.15})O_3$ Ceramics. *Appl. Phys. Lett.* **2017**, *110*, 192903.
(54) Huang, S.; Kim, T.; Hou, D.; Cann, D.; Jones, J. L.; Jiang, X. Flexoelectric Characterization of $BaTiO_3$-0.08$Bi(Zn_{1/2}Ti_{1/2})O_3$. *Appl. Phys. Lett.* **2017**, *110*, 222904.
(55) Zhu, J.; Chen, T.; Shu, L.; Wang, Z.; Huang, W.; Fei, L.; Li, F.; Rao, Z.; Ke, S.; Li, B.; Yao, X.; Wang, Y. Flexoelectric Fatigue in $(K,Na,Li)(Nb,Sb)O_3$ Ceramics. *Appl. Phys. Lett.* **2018**, *113*, 182901.
(56) Li, F.; Zhang, S.; Yang, T.; Xu, Z.; Zhang, N.; Liu, G.; Wang, J.; Wang, J.; Cheng, Z.; Ye, Z. G.; Luo, J.; Shrout, T. R.; Chen, L. Q. The Origin of Ultrahigh Piezoelectricity in Relaxor-Ferroelectric Solid Solution Crystals. *Nat. Commun.* **2016**, *7*, 13807.
(57) Hana, P.; Marvan, M.; Burianova, L.; Zhang, S. J.; Furman, E.; Shrout, T. R. Study of the Inverse Flexoelectric Phenomena in Ceramic Lead Magnesium Niobate-Lead Titanate. *Ferroelectrics* **2011**, *336*, 137−144.
(58) Hana, P. Study of Flexoelectric Phenomenon from Direct and from Inverse Flexoelectric Behavior of PMNT Ceramic. *Ferroelectrics* **2007**, *351*, 196−203.
(59) Tagantsev, A. K. Piezoelectricity and Flexoelectricity in Crystalline Dielectrics. *Phys. Rev. B: Condens. Matter Mater. Phys.* **1986**, *34*, 5883−5889.
(60) Yudin, P. V.; Tagantsev, A. K. Fundamentals of Flexoelectricity in Solids. *Nanotechnology* **2013**, *24*, 432001.
(61) Narvaez, J.; Vasquez-Sancho, F.; Catalan, G. Enhanced Flexoelectric-Like Response in Oxide Semiconductors. *Nature* **2016**, *538*, 219−221.
(62) Biancoli, A.; Fancher, C. M.; Jones, J. L.; Damjanovic, D. Breaking of Macroscopic Centric Symmetry in Paraelectric Phases of Ferroelectric Materials and Implications for Flexoelectricity. *Nat. Mater.* **2015**, *14*, 224−229.
(63) Kim, Y.; Kelly, S. J.; Morozovska, A.; Rahani, E. K.; Strelcov, E.; Eliseev, E.; Jesse, S.; Biegalski, M. D.; Balke, N.; Benedek, N.; Strukov, D.; Aarts, J.; Hwang, I.; Oh, S.; Choi, J. S.; Choi, T.; Park, B. H.; Shenoy, V. B.; Maksymovych, P.; Kalinin, S. V. Mechanical Control of Electroresistive Switching. *Nano Lett.* **2013**, *13*, 4068−4074.
(64) Kong, S.; Kumar, N.; Checchia, S.; Cazorla, C.; Daniels, J. Defect-Driven Structural Distortions at the Surface of Relaxor Ferroelectrics. *Adv. Funct. Mater.* **2019**, *29*, 1900344.
(65) Das, S.; Wang, B.; Paudel, T. R.; Park, S. M.; Tsymbal, E. Y.; Chen, L. Q.; Lee, D.; Noh, T. W. Enhanced Flexoelectricity at Reduced Dimensions Revealed by Mechanically Tunable Quantum Tunnelling. *Nat. Commun.* **2019**, *10*, 537.
(66) Rodriguez, B. J.; Choudhury, S.; Chu, Y. H.; Bhattacharyya, A.; Jesse, S.; Seal, K.; Baddorf, A. P.; Ramesh, R.; Chen, L.-Q.; Kalinin, S. V. Unraveling Deterministic Mesoscopic Polarization Switching Mechanisms: Spatially Resolved Studies of a Tilt Grain Boundary in Bismuth Ferrite. *Adv. Funct. Mater.* **2009**, *19*, 2053−2063.
(67) Glinchuk, M. D.; Eliseev, E. A.; Li, G.; Zeng, J.; Kalinin, S. V.; Morozovska, A. N. Ferroelectricity Induced by Oxygen Vacancies in Relaxors with Perovskite Structure. *Phys. Rev. B* **2018**, *98*, 094102.

DOI: 10.1021/acsami.9b12301
ACS Appl. Mater. Interfaces 2019, 11, 40758−40768